Research Article

Impacts of Air-Sea Energy Transfer on Typhoon Modelling

Difu Sun [ID],[1,2] **Junqiang Song,**[1,2] **Hongze Leng** [ID],[1,2] **Kaijun Ren,**[1,2] **and Xiaoyong Li** [ID][1,2]

[1]*College of Meteorology and Oceanography, National University of Defense Technology, Changsha 410073, China*
[2]*College of Computer Science and Technology, National University of Defense Technology, Changsha 410073, China*

Correspondence should be addressed to Hongze Leng; hzleng@nudt.edu.cn

The Coupled Ocean-Atmosphere-Wave-Sediment Transport model has been used to simulate Super Typhoon Yutu (2018). The impacts of four momentum transfer parameterization schemes (COARE, TY, OT, and DN) and three heat transfer parameterization schemes (COARE, GR, and ZK) on typhoon modelling have been studied by means of the track, intensity, and radial structure of typhoon. The results show that the track of Yutu is not sensitive to the choice of parameterization scheme, while the combinations of different parameterization schemes affect the intensity of Yutu. Among the four momentum flux parameterization schemes, three wave-state-based schemes (TY, OT, and DN) provide better intensity results than the wind-speed-based COARE scheme, but the differences between the three wave-state-based schemes are not obvious. Among the three heat flux parameterization schemes, the results of the GR scheme are slightly better than those of the COARE scheme, and both the GR and COARE schemes are significantly better than the ZK scheme, from which the intensity of Yutu is underpredicted obviously. The influence of the combination of different parameterization schemes on the intensity of the typhoon is also reflected in the radial structure of the typhoon, and the radial structure of the typhoon simulated by experiments with stronger typhoon intensity also develops faster. Differences of intensity between experiments are due mainly to the differences in sea surface heat flux, the enthalpy transferred from sea surface to the atmosphere has a significant impact on the bottom atmosphere wind field, and there is a strong correspondence between the distribution of enthalpy flux and the bottom wind field.

1. Introduction

Tropical cyclones are one of the most severe weather phenomena, which cause huge loss of lives and property to coastal areas [1, 2]. Accurate predictions of the track and intensity of tropical cyclones, especially typhoons and hurricanes, are of great significance for reducing hazards of tropical cyclones and emergency management.

Due to the development of numerical forecasting models, typhoon track forecasts have been greatly improved during the past few decades. However, because of the complexity of the internal physical mechanism of typhoons and the difficulty of accurately describing some small-scale processes related to the intensification of typhoon in numerical forecasting models, the improvement of typhoon intensity forecasting is relatively slow [3].

As the energy source of typhoons, the ocean plays an important role in the generation and intensification of typhoons. An accurate description of the energy exchange between the atmosphere and the ocean is essential to the prediction of typhoon intensity [4–7]. In current models, the energy exchange between the atmosphere and the ocean is described by momentum flux and moist enthalpy flux, where the moisture enthalpy flux is the sum of sensible heat flux and latent heat flux. Momentum flux τ, sensible heat flux SHF, and latent heat flux LHF between air and sea can be expressed as

$$\tau = \rho C_d U_{10}^2, \tag{1}$$

$$\text{SHF} = \rho C_{\text{air}} C_h U_{10} \Delta\theta, \tag{2}$$

$$\text{LHF} = \rho L_{\text{vap}} C_q U_{10} \Delta q, \tag{3}$$

where ρ is the air density, U_{10} is the wind speed at a height of 10 m, C_{air} is the specific heat capacity of air, and L_{vap} is the latent heat of vaporization, C_d, C_h, and C_q are momentum exchange coefficient (also called drag coefficient), sensible

heat flux exchange coefficient, and latent heat flux exchange coefficient, respectively. In neural stratifications, C_d, C_h, and C_q can be calculated from

$$C_d = \frac{k^2}{[\ln(z_{ref}/z_0)]^2}, \tag{4}$$

$$C_h = \frac{k^2}{\ln(z_{ref}/z_0) \times \ln(z_{ref}/z_t)}, \tag{5}$$

$$C_q = \frac{k^2}{\ln(z_{ref}/z_0) \times \ln(z_{ref}/z_q)}, \tag{6}$$

where $k = 0.4$ is the Von Kármán constant, z_{ref} is the reference height, often taken as 10 m, z_0, z_t, and z_q are the roughness length for momentum, sensible heat, and water vapor, respectively.

For the calculation of momentum flux, early applications treated C_d or z_0 as a function of wind speed. In low and moderate wind conditions ($U_{10} \leq 20 m/s$), many observations show that C_d increases linearly with wind speed [8–10]. Therefore, the function of C_d in low and moderate wind conditions can be expressed as

$$10^3 C_d = a + b U_{10}. \tag{7}$$

From different observations, the coefficients a and b are fitted to different values (Table 1). It can be seen that the functions of C_d fitted by different observations all reveal the monotonically increasing relationship of C_d with U_{10}, but the values of coefficients a and b differ significantly. The difference indicates that C_d may not only depend on wind speed. Many studies have shown that wave state has an important influence on the surface roughness [11, 12].

Due to the lack of observations under high wind speed conditions, in some early models [21, 22], the linear relation between C_d and U_{10} is extrapolated to high wind speed conditions. However, some recent field experiments and laboratory experiments show that when the wind speed reaches a certain level, C_d no longer increases with the increase of U_{10}, but reaches a saturation value [23, 24], or decreases with the increase of U_{10} [25]. This C_d saturation effect is related to the wave breaking and the generation of sea foam under high wind speeds [26, 27]. Due to the important influence of wave state on momentum transfer, many wave-state-based sea surface roughness parameterization schemes have been proposed to calculate the momentum flux between air and sea, such as the wave-steepness-based z_0 parameterization scheme proposed by Taylor and Yelland [28] (equation (8)) and the wave-age-based scheme proposed by Drennan et al. [29] (equation (9)):

$$\frac{z_0}{H_s} = 1.2 \times 10^2 \left(\frac{H_s}{L_p}\right)^{4.5}, \tag{8}$$

$$\frac{z_0}{H_s} = 3.35 \times \left(\frac{c_p}{u_*}\right)^{-3.4}, \tag{9}$$

Table 1: Coefficients a and b in (7) from various observations.

Reference	a	b
Kondo [13]	1.20	0.025
Wu [14]	0.80	0.065
Large and Pond [15]	0.49	0.065
Donelan [16]	0.96	0.041
Geernaert et al. [9]	0.58	0.085
Vickers and Mahrt [17]	0.75	0.067
Drennan et al. [18]	0.60	0.070
Guan and Xie [19]	0.78	0.065
Toffoli et al. [20]	0.96	0.060

where H_s is the significant wave height, L_p is the wave length at the spectral peak, H_s/L_p denotes the wave steepness, c_p is the wave speed at the spectral peak, u_* is the friction velocity, and c_p/u_* denotes the wave age. Compared with the scheme based on wind speed, schemes based on wave state describe the physical state of the sea surface more directly and are often used in the atmosphere-ocean-wave coupling model, in which the wave state is provided by the ocean model or the wave model.

The heat transported from ocean to atmosphere is the main energy source for typhoon [30, 31]. Due to the difficulties in measuring heat flux directly, the mechanism of air-sea heat transfer is relatively dubious. According to the method adopted, the parameterization schemes of heat flux can be roughly divided into the following categories: (1) based on the observations in low and moderate wind conditions, sensible heat flux exchange coefficient C_h and latent heat flux exchange coefficient C_q are treated as a constant [32]; (2) by fitting observations directly to dimensionless parameters, such as roughness Reynolds number R_r, the sensible heat roughness z_t and water vapor roughness z_q can be denoted as a function of dimensionless parameters [33]; (3) describe the ratio between z_t or z_q and z_0 as a function of roughness Reynolds number R_r and Prandtl number P_r: $z_{t,q} = f(R_r, P_r)$ [34]. As mentioned above, there are differences between different heat flux parameterization schemes, which will lead to differences in the typhoon modelling results.

This study aims to improve the understanding of the influence of air-sea energy exchange on typhoon modelling, especially the influence on intensity forecast. To examine the impact of momentum flux and heat flux on typhoon intensity, we evaluated the performance of four momentum flux parameterization schemes and three heat flux parameterization schemes in the simulation of Super Typhoon Yutu.

2. Methods

2.1. Momentum Flux Parameterization Schemes. In the numerical model, the momentum flux of the sea surface is determined by the drag coefficient C_d (equation (1)), and C_d can be calculated from z_0 (equation (4)). Therefore, different momentum flux parameterization schemes in the model are realized by different calculation schemes for z_0.

2.1.1. COARE. COARE (Coupled Ocean-Atmosphere Response Experiment) scheme was proposed based on the flux measurements collected from the TOGA (Tropical Ocean Global Atmosphere) COARE experiment [35], which is widely used in flux calculations in various numerical models [36, 37]; here we adopt the v3.5 version of COARE proposed by Edson et al. [10].

COARE divides z_0 into two parts:

$$z_0 = z_0^{\text{smooth}} + z_0^{\text{rough}}, \tag{10}$$

where z_0^{smooth} represents the roughness corresponding to the part of the momentum transported entirely by the viscous effect of the sea surface when the sea surface is flat; in addition to the momentum transfer caused by the viscous effect, due to the actual unevenness of the sea surface, the wind produces horizontal wind pressure on the sea surface, which causes the horizontal momentum to be transferred to waves, and this part of the momentum transfer corresponds to roughness z_0^{rough}. z_0^{smooth} is calculated from

$$z_0^{\text{smooth}} = \gamma \frac{\nu}{u_*}, \tag{11}$$

where ν is the kinematic viscosity of air and γ is taken as 0.11 by COARE from observations. z_0^{rough} is often calculated from Charnock relation [38]:

$$z_0^{\text{rough}} = \alpha \frac{u_*^2}{g}, \tag{12}$$

where α is the Charnock coefficient and g is the gravitational acceleration. Then, (10) is written as

$$z_0 = \gamma \frac{\nu}{u_*} + \alpha \frac{u_*^2}{g}. \tag{13}$$

Charnock coefficient α is denoted as a function of wind speed by COARE based on observations:

$$\alpha = mU_{10} + b, \tag{14}$$

where $m = 0.017 \, \text{m}^{-1}\text{s}$ and $b = -0.005$.

2.1.2. TY. Based on the observations from HEXOS (the Humidity Exchange over the Sea) [39], RASEX (the Risø Air-Sea Exchange) [40], and Lake Ontario [41] experiments, Taylor and Yelland [28] proposed a sea surface roughness parameterization scheme considering significant wave height H_s and wave steepness H_s/L_p:

$$\frac{z_0}{H_s} = 1200 \left(\frac{H_s}{L_p} \right)^{4.5}. \tag{15}$$

Compared with the wind-speed-based COARE scheme, TY scheme describes the relationship between the physical properties of the sea surface and z_0 more directly.

2.1.3. OT. From the momentum flux observations collected from ASGMAGE (an union of ASGASEX (Air Sea GAS

EXchange) and MAGE (Marine Aerosol and Gas Exchange)) experiment, Oost et al. [42] proposed a scheme considering wave length L_p and wave age c_p/u_*:

$$\frac{z_0}{L_p} = \frac{25}{\pi} \left(\frac{u_*}{c_p} \right)^{4.5}, \tag{16}$$

Wave age c_p/u_* represents the relative magnitude of wave speed and wind speed, and the ability of winds to transfer momentum to waves.

2.1.4. DN. By filtering out momentum flux data from the pure wind wave field and deep water conditions from AGILE (measured from the 15-m research vessel *AGILE*) [43], FETCH (Flux, sea state, and remote sensing in conditions of variable fetch) [44], HEXOS, SWADE (Surface Waves Dynamics Experiment) [45], and WAVES (Water-Air Vertical Exchange Study) [46] experiments, Drennan et al. [29] proposed a scheme considering wave age c_p/u_*:

$$\frac{z_0}{H_s} = 3.35 \left(\frac{u_*}{c_p} \right)^{3.4}. \tag{17}$$

Among the above four schemes, except for the COARE scheme, which uses wind speed to calculate z_0, the other three schemes are all based on wave parameters. Since the atmospheric model generally does not directly provide wave parameters, TY, OT, and DN schemes are mainly used in the coupled model, in which the wave parameters can be provided by wave model.

2.2. Heat Flux Parameterization Schemes

2.2.1. COARE. In addition to the calculation scheme of z_0, COARE also provides the calculation scheme of z_t and z_q. In COARE scheme, z_t and z_q are taken as the same value:

$$z_t = z_q = \min\left(1.6 \times 10^{-4}, \, 5.5 \times 10^{-5} R_r^{-0.6}\right), \tag{18}$$

where $R_r = z_0 u_*/\nu$ is the roughness Reynolds number.

2.2.2. GR. GR scheme proposed by Garratt [47] calculate z_t and z_q from z_0 and R_r; values of z_t and z_q are slightly different:

$$
\begin{aligned}
z_t &= z_0 \exp\left(2 - 2.48\left(R_r^{1/4}\right)\right), \\
z_q &= z_0 \exp\left(2 - 2.28\left(R_r^{1/4}\right)\right).
\end{aligned}
\tag{19}
$$

2.2.3. ZK. Based on the observations from TOGA COARE and SCOPE (San Clemente Ocean Probing Experiment) [48], Zilitinkevich et al. [34] proposed a scheme to calculate z_t and z_q in different sea surface roughness conditions:

$$z_t = \begin{cases} z_0 \exp\left(k \times 2.0\right), & R_r < 0.1 \\ z_0 \exp\left(-k \times \left(4.0 R_r^{1/2} - 3.2\right)\right), & R_r \geq 0.1 \end{cases},$$

$$z_q = \begin{cases} z_0 \exp\left(k \times 3.0\right), & R_r < 0.1 \\ z_0 \exp\left(-k \times \left(4.0 R_r^{1/2} - 4.2\right)\right), & R_r \geq 0.1 \end{cases} \tag{20}$$

$R_r = 0.1$ is chosen as the threshold value because the fitting curves of observational data match the curves of smooth regime equations at that point.

2.3. Evaluation Parameters.

2.3. Evaluation Parameters. To quantitatively compare the results of the typhoon simulations, we introduced three parameters to evaluate the simulation results: the root mean square error (RMSE), Pearson correlation coefficient (R), and model skill (S), given as

$$\text{RMSE} = \sqrt{\frac{1}{N} \sum_{i=1}^{N} (y_i - x_i)^2},$$

$$R = \frac{\sum_{i=1}^{N} (y_i - \overline{y})(x_i - \overline{x})}{\sqrt{\sum_{i=1}^{N} (x_i - \overline{x})^2} \sqrt{\sum_{i=1}^{N} (y_i - \overline{y})^2}}, \tag{21}$$

$$S = 1 - \frac{\sum_{i=1}^{N} |y_i - x_i|^2}{\sum_{i=1}^{N} \left(|y_i - \overline{x}|^2 + |x_i - \overline{x}|^2\right)},$$

where x_i and y_i represent the observed and simulated values, respectively, with respect to time.

3. Case Introduction and Experimental Design

3.1. An Overview of Super Typhoon Yutu. Super Typhoon Yutu is the 26th named tropical cyclone in the Western North Pacific in 2018. At 1200 UTC 21 Oct 2018, Yutu formed as a tropical depression on the tropical ocean near 158°E and 8°N, it upgraded to a tropical storm at 0000 UTC 22 Oct, and then it reached the intensity of typhoon at 0000 UTC 23 Oct. At 2000 UTC 24 Oct, its intensity exceeded the Super Typhoon Mangkhut (22nd named tropical cyclone in the Northwest Pacific in 2018) and thus became the strongest tropical cyclone in 2018. Figure 1 shows the track and intensity changes of Yutu from the Best-Track data released by the JTWC (Joint Typhoon Warning Center).

3.2. Experimental Design. Experiments in this study are conducted on the COAWST (Coupled Ocean–Atmosphere-Wave-Sediment Transport) [49] model. Super Typhoon Yutu is simulated in the atmospheric model, and wave model is activated to provide wave parameters to atmospheric model for the calculation of z_0, because the activation of ocean model will cause a cold deviation of the sea surface temperature in the simulation of tropical cyclones over the Western North Pacific [50], and the ocean model was not activated in our experiments.

Weather Research and Forecasting (WRF-ARW 4.1.5) model is the atmospheric model used in the coupled model.
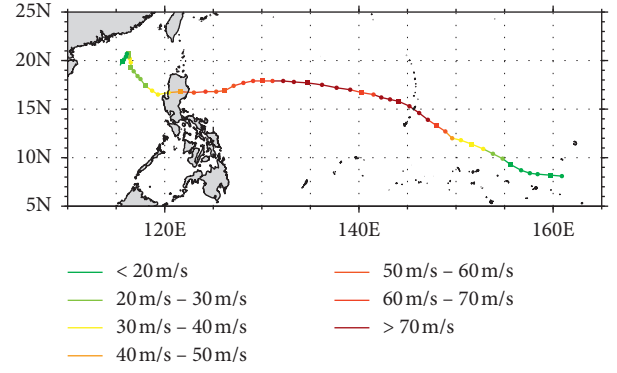

Figure 1: Intensity and track of Yutu from JTWC Best-Track data between 1800 UTC 20 Oct 2018 and 0600 UTC 3 Nov 2018. Positions at 0000 UTC are marked by squares, and the colors of the track indicate the maximum wind speed at 10 m level above the sea surface.

6-hourly $0.25° \times 0.25°$ GDAS (Global Data Assimilation System) Final Analysis data from NCEP (National Centers for Environmental Prediction) were used as the initial and boundary conditions. There are three two-way nested grids in the present work-D01, D02, and D03 (Figure 2). The outermost grid D01 has a horizontal spacing of 27 km and a time step of 90 s; the second grid D02 has a horizontal spacing of 9 km and a time step of 30 s; the innermost grid D03 is a vortex following grid moving along the typhoon center, the vortex is tracked at 500 hPa level, its position is calculated every 15 minutes, and the max vortex speed is taken as 40 m/s for the calculation of the new vortex center position; its initial position is drawn as the red box in Figure 2, the horizontal spacing of D03 is 3 km, and its time step is 10 s. A total of 44 vertical layers with a pressure top of 10 hPa are adopted. Purdue Lin's [51] scheme is used as the microphysics scheme; both shortwave and longwave radiation are resolved by Rapid Radiative Transfer Model for Global Circulation Models (RRTMG) [52], Mellor-Yamada Nakanishi and Niino level 2.5 (MYNN) [53] is adopted as the planetary boundary layer scheme, surface layer model is MYNN, land surface model is set to Unified Noah [54], and Kain-Fritsch [55] cumulus scheme is only activated in D01 and D02.

Wave parameters needed (H_s, L_p, and c_p) in the calculation of z_0 are calculated by wave model SWAN (Simulating Waves Nearshore, 41.31) and are transferred to WRF through the coupler MCT (Model Coupling Toolkit); SWAN model also receives the 10 m wind field from WRF as the forcing field. Horizontal spacing of SWAN is about 9 km, and the time step is 180 s; the domain of SWAN is shown as the blue box in Figure 2.

Both atmospheric and wave model are initialized at 1200 UTC 22 Oct 2018 and are integrated for 5 days to 1200 UTC 27 Oct 2018. The simulation period covers the entire enhancement process of Yutu; in this period, track of Yutu is all over the sea, and the influence of different parameterization schemes on the momentum and heat transfer between ocean and typhoon can be fully analysed.
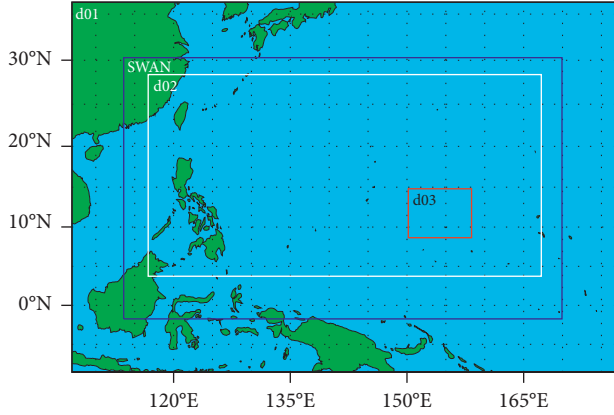
Figure 2: Model domains configuration. The outermost is the domain of D01, the white box represents the domain of D02, the red box represents the initial position of vertex-following nest D03, and the blue box represents the domain of SWAN.

Table 2: Parameterization schemes of momentum and heat flux in 12 experiments.

EXP ID	EXP name	Momentum flux scheme	Heat flux scheme
1	CR_CR	COARE	COARE
2	CR_GR	COARE	GR
3	CR_ZK	COARE	ZK
4	TY_CR	TY	COARE
5	TY_GR	TY	GR
6	TY_ZK	TY	ZK
7	OT_CR	OT	COARE
8	OT_GR	OT	GR
9	OT_ZK	OT	ZK
10	DN_CR	DN	COARE
11	DN_GR	DN	GR
12	DN_ZK	DN	ZK

There are 12 experiments in this study: four momentum flux parameterization schemes and three heat flux parameterization schemes described in Section 2 are called pairwise. Except for the flux parameterization scheme, other settings are all the same. The parameterization schemes used in each group of experiments are summarized in Table 2.

4. Results and Discussion

4.1. Track and Intensity. Comparison between simulated tracks of Yutu and Best-Track data is plotted in Figure 3. Overall, the movement of typhoon from the southeast to the northwest is reproduced by every experiment, but the simulated moving speeds are slower than that of the Best-Track data. Differences of tracks between 12 experiments are not obvious, and the tracks of Yutu before 0000 UTC 25 Oct from 12 experiments are generally the same. In general, simulated tracks of Yutu are not sensitive to the flux parameterization schemes, which is in agreement with many typhoon simulation studies [3, 56], because typhoon track is mainly affected by the large-scale steering flow, while the small-scale flux transport has limited impact on it.

Comparisons between simulated intensities and Best-Track data are shown in Figure 4. Results of MSLP (minimum sea level pressure) are plotted in Figure 4(a). From the Best-Track data, we can see that Yutu intensified rapidly during 12–48 h of the simulation period, and its MSLP reduced by about 80 hPa, but this rapid intensification process has not been reproduced well by experiments; the reduction speeds of simulated MSLP are slower than that of Best-Track data. Although the mechanism of the rapid intensification of tropical cyclone is still controversial [57], it is widely accepted that the thermodynamic and kinematic properties of the TC core play an important role in rapid intensification [58, 59]. In the numerical simulations, how the model calculates convective process matters a lot for the rapid intensification of TC. Hence, the failure in reproducing the rapid intensification of Yutu may be due to the inability of the current convection calculation

scheme to reproduce the convection processes in the TC core. Results simulated by different experiments differ a lot; MSLP from four experiments using ZK scheme as the heat flux parameterization scheme (CR_ZK, TY_ZK, OT_ZK, and DN_ZK) is much larger than others, which denotes the typhoon intensities are affected by the adoptions of ZK scheme. The performances of COARE, GR, and ZK schemes in numerical simulations have also been evaluated by Bao et al. [4] using the National Atmospheric and Oceanic Administration/ Environmental Technology Laboratory (NOAA/ETL) regional air-sea coupled modelling system, from their results (Figure 1 in Bao et al. [4]). ZK scheme showed the worst performances, hurricane simulated by ZK scheme did not intensify at all, and GR scheme was slightly better than COARE scheme. Due to the different MSLP reduction speeds simulated by different experiments, the simulation results of MSLP showed a big difference at 120 h: the smallest is about 900 hPa (DN_CR) and the largest is about 940 hPa (CR_ZK); the difference exceeds 40 hPa.

Figure 4(b) presents the results of UMAX (maximum wind speed at 10 m level); the increasing trend of UMAX corresponds to the decreasing trend of MSLP, the rapid increasing of UMAX during 12–48 h is also not reproduced well by experiments, and UMAX simulated by the four experiments using ZK scheme as the heat flux parameterization scheme also showed obvious weak deviations.

Listed in Table 3 are the RMSE, Pearson correlation coefficient, and model skill of simulated MSLP from 12 experiments. Among the 12 experiments, RMSE of TY_CR is the smallest (17.30 hPa), and the largest is that of CR_ZK (34.49 hPa). The difference in Pearson correlation coefficient between different experiments is not obvious. The model skill also shows significant differences: the highest is TY_CR (0.8447) and the lowest is CR_ZK (0.4198), which is consistent with the results of RMSE.

To compare the performances of different parameterization schemes on MSLP simulation more intuitively, Table 4 lists the average RMSE, R, and S of experiments that use the same schemes. From the results of four momentum flux parameterization schemes, it can be seen that the performance of wave –state-based TY, OT, and DN schemes is generally better than the wind-speed-based COARE scheme.
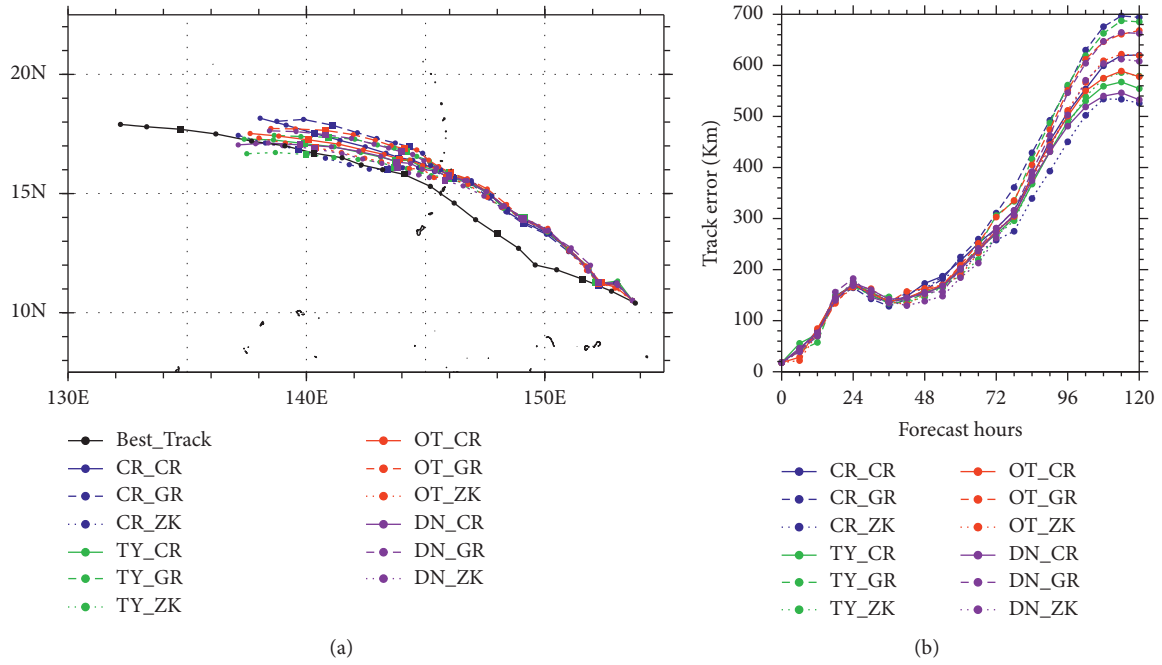
Figure 3: Simulated (a) tracks between 1200 UTC 22 Oct 2018 and 1200 UTC 27 Oct 2018 (positions at 0000 UTC are marked by squares) and (b) track errors from different experiments.
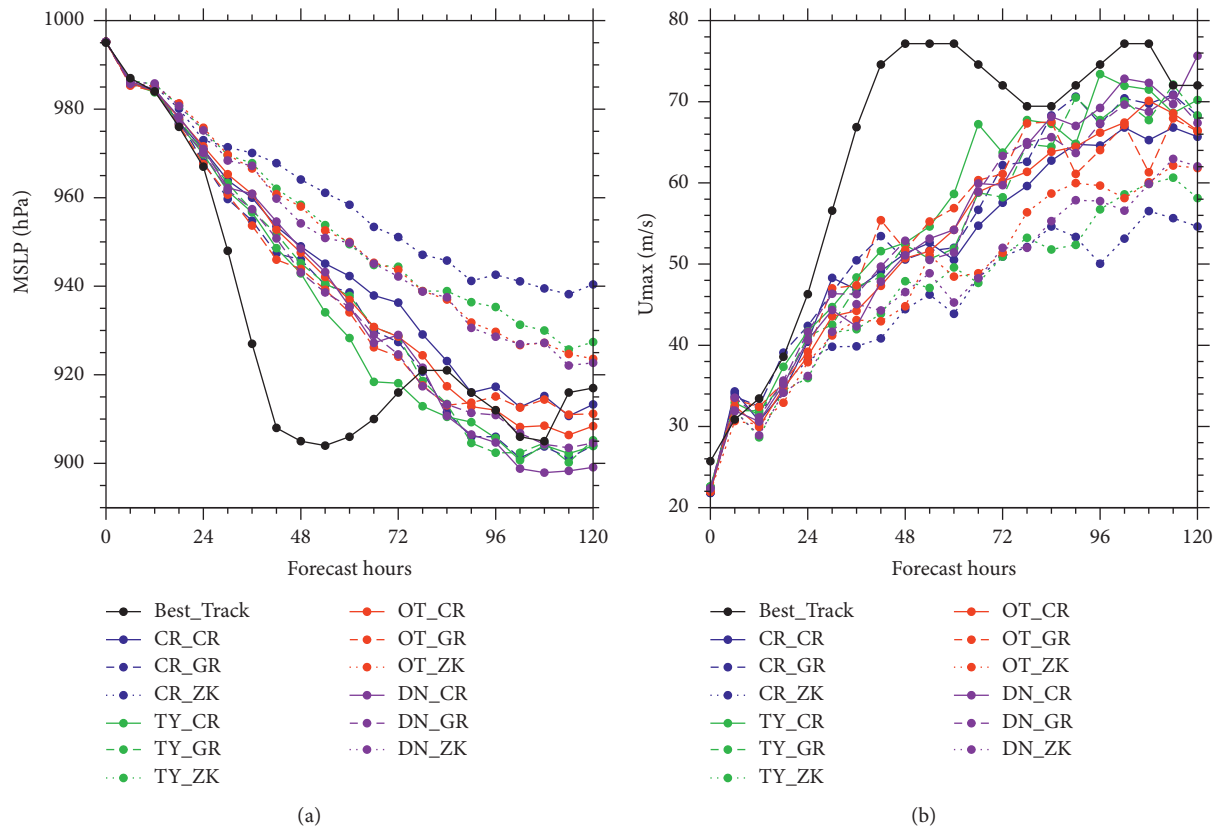

Figure 4: Comparison between Yutu's JTWC Best-Track data and simulated intensities (a) for minimum sea level pressure and (b) for maximum wind speed at 10 m level above the sea surface.

TABLE 3: Root mean square error (RMSE), Pearson correlation coefficient (R), and model skill (S) for MSLP from 12 experiments.

EXP name	RMSE (hPa)	R	S
CR_CR	21.66	0.8378	0.7461
CR_GR	19.14	0.8340	0.8077
CR_ZK	34.49	0.8241	0.4198
TY_CR	17.30	0.8603	0.8447
TY_GR	19.90	0.8243	0.7956
TY_ZK	28.83	0.8449	0.5661
OT_CR	20.13	0.8390	0.7838
OT_GR	17.55	0.8740	0.8259
OT_ZK	27.81	0.8361	0.5938
DN_CR	21.03	0.8065	0.7802
DN_GR	18.65	0.8470	0.8145
DN_ZK	27.03	0.8441	0.6125

TABLE 4: Averaged root mean square error (RMSE), Pearson correlation coefficient (R), and model skill (S) for MSLP from different schemes.

Group	RMSE (hPa)	R	S
COARE momentum flux scheme group averaged (CR_CR, CR_GR, and CR_ZK)	25.10	0.8320	0.6564
TY momentum flux scheme group averaged (TY_CR, TY_GR, and TY_ZK)	22.01	0.8432	0.7355
OT momentum flux scheme group averaged (OT_CR, OT_GR, and OT_ZK)	21.83	0.8497	0.7345
DN momentum flux scheme group averaged (DN_CR, DN_GR, and DN_ZK)	22.24	0.8325	0.7357
COARE heat flux scheme group averaged (CR_CR, TY_CR, OT_CR, and DN_CR)	20.03	0.8434	0.7876
GR heat flux scheme group averaged (CR_GR, TY_GR, OT_GR, and DN_GR)	18.81	0.8448	0.8109
ZK heat flux scheme group averaged (CR_ZK, TY_ZK, OT_ZK, and DN_ZK)	29.54	0.8373	0.5481

Compared with the COARE scheme, RMSE of MSLP simulated by three wave-state-based momentum flux parameterization schemes is reduced by about 3 hPa on average. COARE is one of the best wind-speed-based z_0 parameterization schemes, which has been widely used in momentum flux calculations [60, 61]; the better results from wave-state-based schemes reveal that the characteristics of momentum flux at typhoon condition are better captured by the wave-state-based schemes; this denotes that considering the impacts of wave state can provide more information for the parameterization of z_0. Similar conclusions are presented by Drennan et al. [62] and Prakash et al. [63]. From the results of three heat flux parameterization schemes, it is demonstrated that the MSLP results simulated by the ZK scheme are worse than the other two schemes. The MSLP RMSE is significantly higher, and the model skill is significantly lower. Results of the GR scheme are slightly better than the COARE scheme. The relative performances of three heat flux parameterization schemes are consistent with Bao et al. [4].

RMSE, Pearson correlation coefficient, and model skill of simulated UMAX from 12 experiments are given in Table 5. Among 12 experiments, RMSE of TY_CR is the smallest (11.47 m/s), and the largest is that of CR_ZK (21.35 m/s). Results of model skill are similar to RMSE; the highest is TY_CR (0.7725), and the lowest is CR_ZK (0.3624). Table 6 lists the group averaged root mean square error (RMSE), Pearson correlation coefficient (R), and model skill (S). From the results of four momentum flux parameterization schemes, it can be seen that the performance of wave-state-

TABLE 5: Root mean square error (RMSE), Pearson correlation coefficient (R), and model skill (S) for UMAX from 12 experiments.

EXP name	RMSE (m/s)	R	S
CR_CR	14.67	0.8724	0.6465
CR_GR	12.88	0.8480	0.7094
CR_ZK	21.35	0.8383	0.3624
TY_CR	11.47	0.8803	0.7725
TY_GR	13.74	0.8440	0.6870
TY_ZK	19.37	0.8847	0.4562
OT_CR	14.15	0.8668	0.6737
OT_GR	12.76	0.8996	0.7149
OT_ZK	18.36	0.8524	0.4999
DN_CR	13.49	0.8337	0.7064
DN_GR	13.43	0.8545	0.6928
DN_ZK	18.91	0.8580	0.4743

based schemes (TY, OT, and DN) is generally better than the wind-speed-based scheme (COARE), which are consistent with the results in Table 4. RMSE of UMAX simulated by TY, OT, and DN is 1.2 m/s smaller than COARE on average. By comparing the results of COARE, GR, and ZK, it is demonstrated that the UMAX results simulated by the ZK scheme are worse than the other two schemes; results of the GR scheme are slightly better than the COARE scheme.

4.2. Time Evolution of Radial Structure. To analyse the time evolution of the typhoon radial structure, the Hovmöller diagrams of azimuthally averaged SLP (sea level pressure) and U_{10} are plotted in Figures 5 and 6, respectively. The

TABLE 6: Averaged root mean square error (RMSE), Pearson correlation coefficient (R), and model skill (S) for UMAX from different schemes.

Group	RMSE (m/s)	R	S
COARE momentum flux scheme group averaged (CR_CR, CR_GR, and CR_ZK)	16.30	0.8529	0.5728
TY momentum flux scheme group averaged (TY_CR, TY_GR, and TY_ZK)	14.86	0.8697	0.6386
OT momentum flux scheme group averaged (OT_CR, OT_GR, and OT_ZK)	15.09	0.8729	0.6295
DN momentum flux scheme group averaged (DN_CR, DN_GR, and DN_ZK)	15.27	0.8487	0.6245
COARE heat flux scheme group averaged (CR_CR, TY_CR, OT_CR, and DN_CR)	13.45	0.8633	0.6998
GR heat flux scheme group averaged (CR_GR, TY_GR, OT_GR, and DN_GR)	13.20	0.8615	0.7010
ZK heat flux scheme group averaged (CR_ZK, TY_ZK, OT_ZK, and DN_ZK)	19.50	0.8584	0.4482
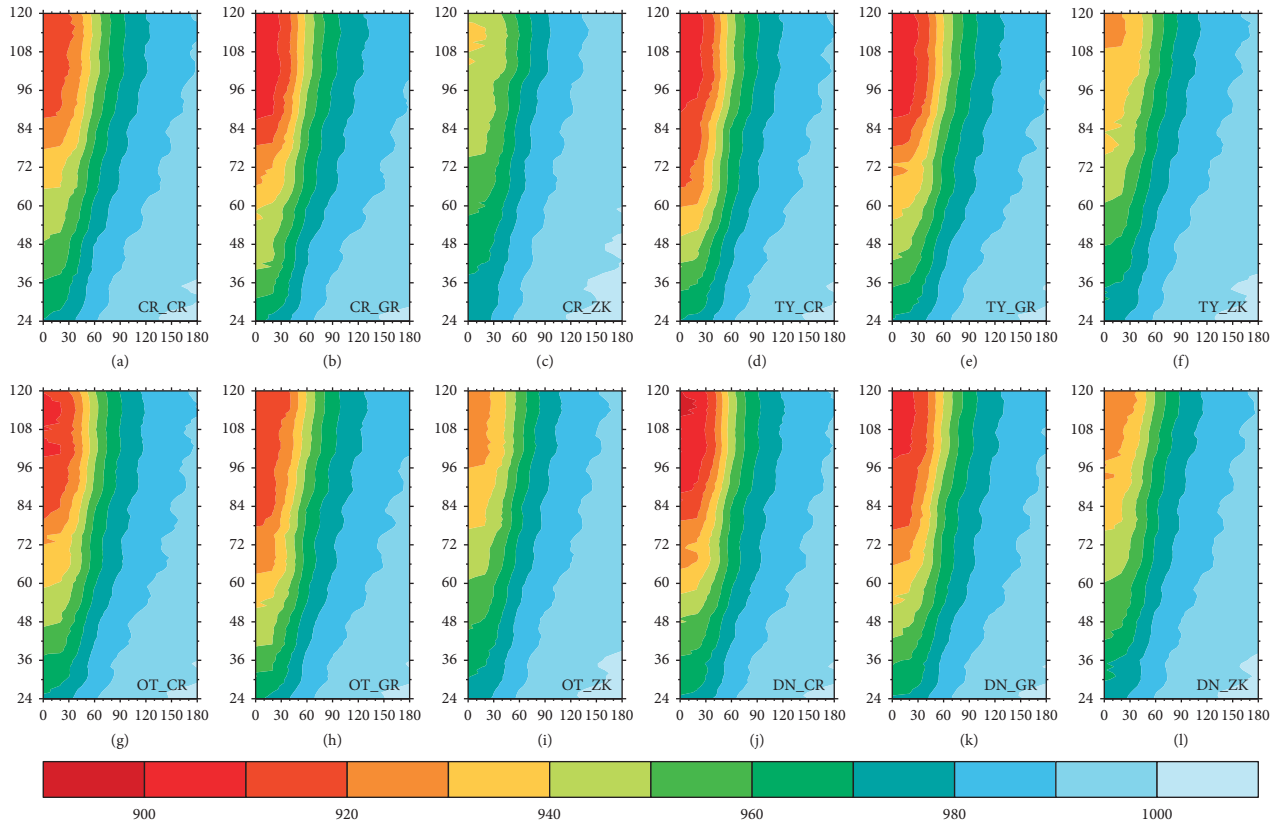
FIGURE 5: Hovmöller diagrams of azimuthally averaged sea level pressure (hPa) from 12 experiments. x-axis denotes the distance (km) from the center of the typhoon and y-axis denotes the forecast hours.

intensification and the structure development of typhoon are presented in Figure 5; results in Figure 5 are consistent with the results in section 4.1, and experiments using ZK as the heat flux parameterization scheme tend to underestimate the intensity of Yutu. The faster the typhoon intensifies, the faster the radial pressure gradient increases. Here we take CR_ZK (Figure 5(c)) and TY_CR (Figure 5(d)) as examples. Typhoon simulated by TY_CR intensifies rapidly; it takes 42 h for TY_CR to intensify to 950 hPa, while typhoon simulated by CR_ZK intensifies slower, and it takes about 75 h for CR_ZK to intensify to 950 hPa; in addition to the difference in the speed of the central pressure drop, the development speed of their radial structure is also significantly different. At 72 h, the 980 hPa isobar of CR_ZK is located about 70 km from the center of typhoon, while the

980 hPa isobar of TY_CR is located about 90 km from the center of typhoon, indicating that the radial structure simulated by TY_CR is stronger. It is worth mentioning that typhoon structure simulated by the four experiments that use the ZK heat flux parameterization scheme (CR_ZK (Figure 5(c)), TY_ZK (Figure 5(f)), OT_ZK (Figure 5(j)), and DN_ZK (Figure 5(l)) is not sufficiently developed, which is consistent with the results in Section 4.1.

Figure 6 shows the time evolution of azimuthally averaged tangential winds and radial winds. It can be seen that the wind speeds are relatively small near the center and reaches the maximum value as radius increases and then decreases with radius. The values of tangential winds can reach to more than 50 m/s, while the maximum value of radial winds is only 25–30 m/s, indicating that the bottom
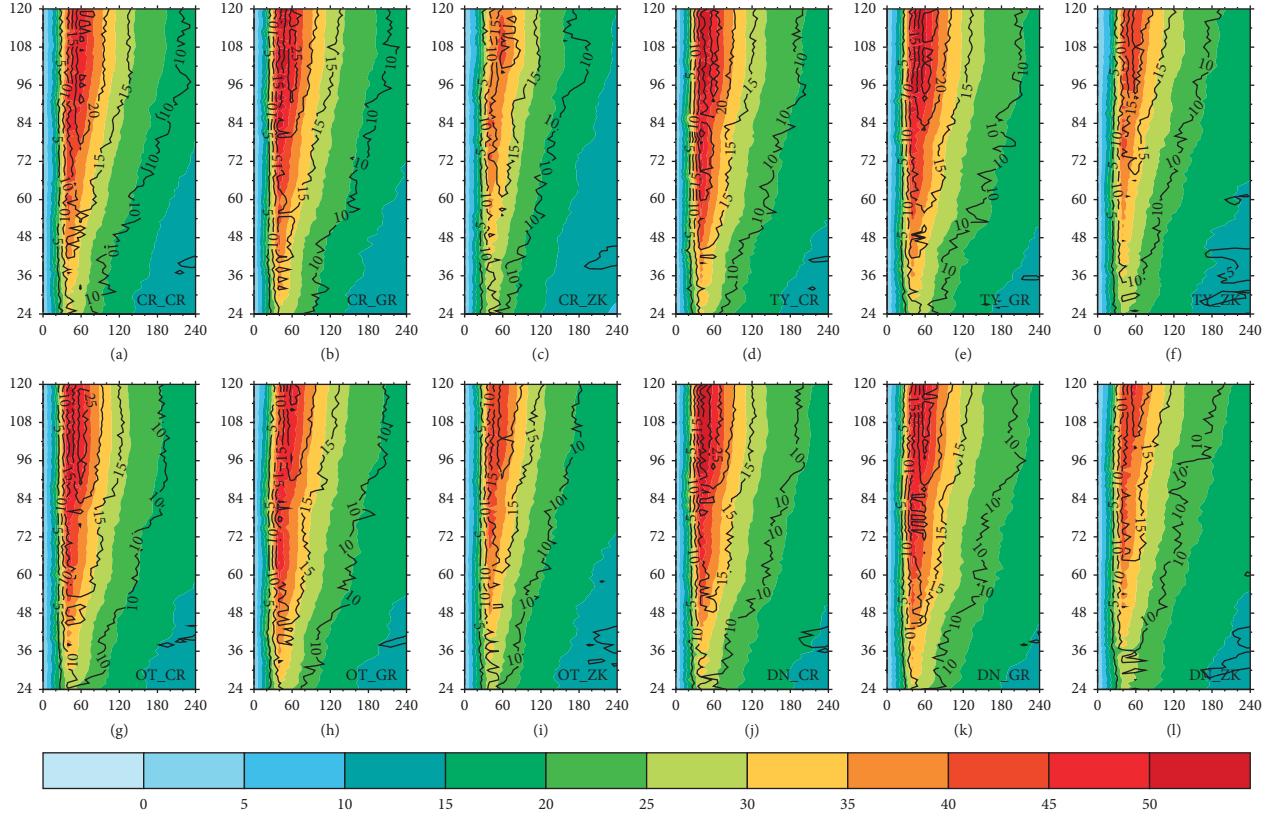
FIGURE 6: Hovmöller diagrams of azimuthally averaged tangential winds (colors, m/s) and radial winds (black lines, m/s) from 12 experiments. x-axis denotes the distance (km) from the center of the typhoon and y-axis denotes the forecast hours.
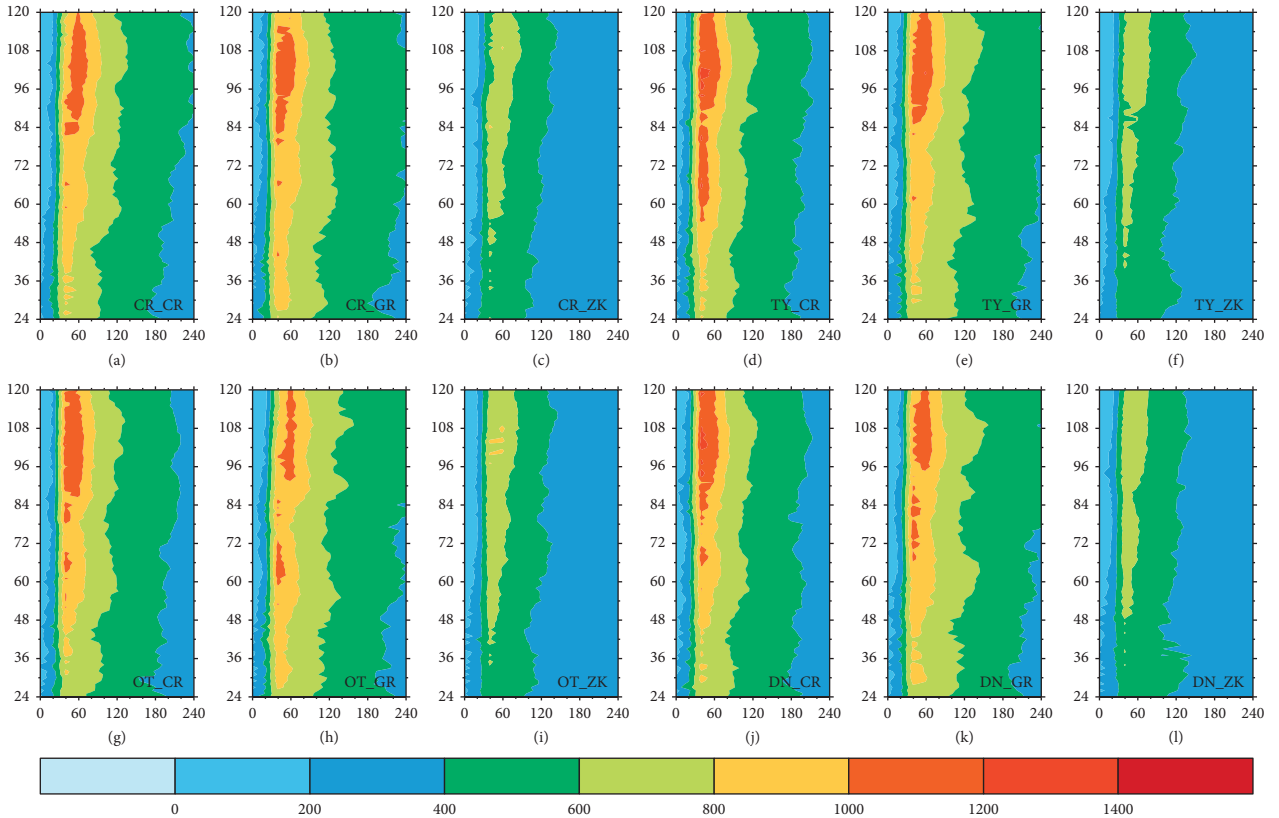

FIGURE 7: Hovmöller diagrams of azimuthally averaged latent heat flux (W/m^2) from 12 experiments. x-axis denotes the distance (km) from the center of the typhoon and y-axis denotes the forecast hours.
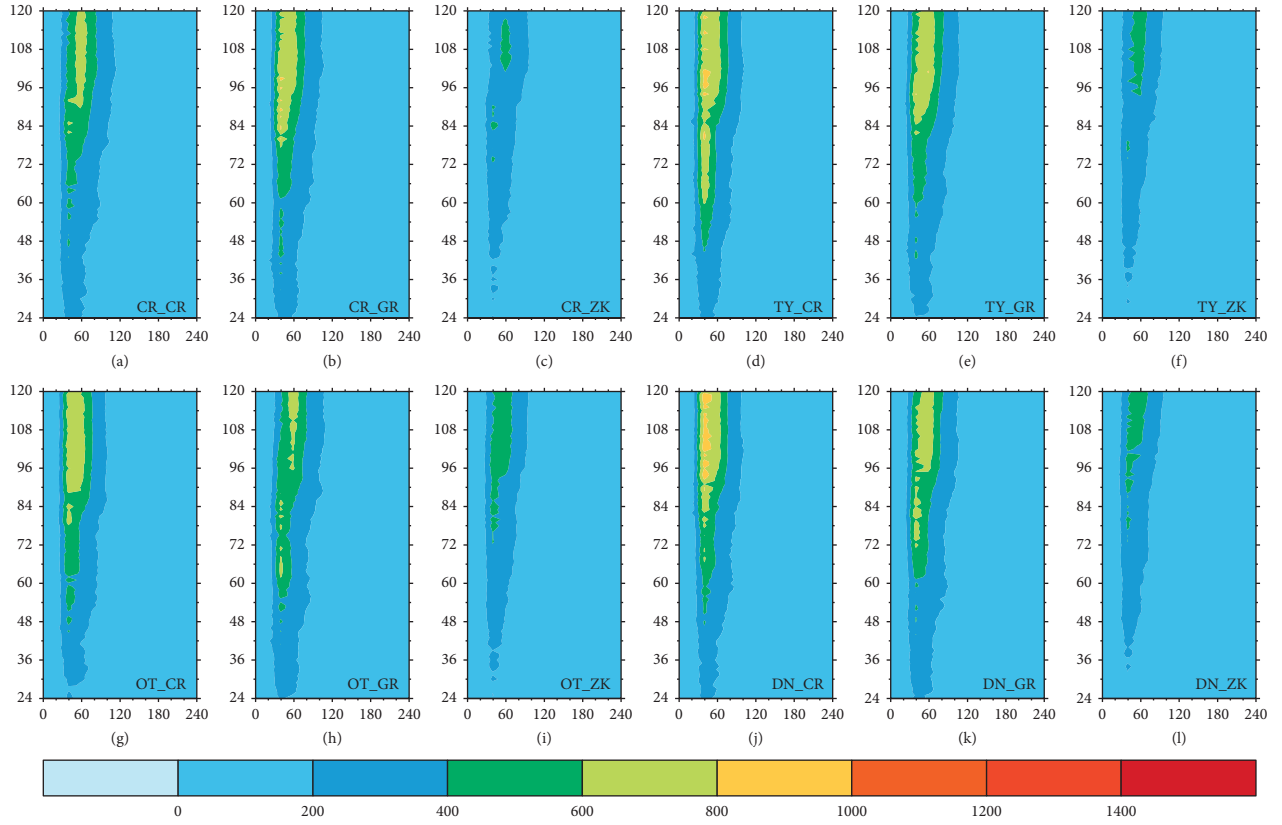
FIGURE 8: As in Figure 7, but for the azimuthally averaged sensible heat flux (W/m^2).

wind field structure of a typhoon is dominated by tangential rotation, accompanied by a weaker convergence effect. The maximum value of radial wind generally appears at a distance of 60 km from the center, while the maximum value of tangential wind is probably distributed between 40 and 60 km, indicating that the region with strongest convergence effect is slightly outside the region with the strongest rotation effect. This feature has also been presented by Green and Zhang [6] (see Figure 7 therein). From the results of experiments with strong typhoon intensity (CR_GR (Figure 6(b)), TY_CR (Figure 6(d)), TY_GR (Figure 6(e)), OT_CR (Figure 6(g)), and DN_CR (Figure 6(j)), the maximum tangential wind speed radius at 120 h is roughly 40–50 km, while for experiments with weaker typhoon intensity (CR_ZK (Figure 6(c)) and DN_ZK (Figure 6(l)), the maximum tangential wind speed radius at 120 h is about 60 km, indicating that not only the horizontal scale of typhoon, but also the radial distributions of winds are affected by momentum and heat transfer between air and sea.

4.3. Heat Flux at Sea Surface. To determine the causes of differences in typhoon intensity from different experiments, we analysed the heat flux at sea surface simulated by different experiments. Time evolution of azimuthally averaged latent heat flux and sensible heat flux at sea surface is plotted in Figures 7 and 8, respectively. By comparison, heat transported by latent heat flux is stronger than the sensible heat flux. Similar to the distribution of wind speed in Figure 6, the

distributions of two heat fluxes both show the characteristics of increasing at first, and then decreasing along the radial direction. Heat transfer in Figures 7 and 8 corresponds to the development of wind field in Figure 6, and typhoon simulated by experiments with stronger heat flux can acquire more energy from the ocean, which lead to the development of wind field. The poor results from ZK scheme in the intensity simulation are caused by the poor results in the calculation of heat flux, which are caused by the unreasonable calculation of z_t and z_q. The enthalpy exchange coefficient calculated by ZK decreases with increasing wind speed (cf Figure 2(b) in Bao et al. [4]), which is not consistent with the consensus that enthalpy exchange coefficient increases or keeps constant with increasing wind speed [64–66].

To verify this result, we plotted the distribution of enthalpy flux (sum of latent heat flux and sensible heat flux) and 10 m level wind speed at 120 h (1200 UTC 27 Oct 2018) in Figure 9. It is demonstrated that there is a strong correlation between distributions of wind speed and distributions of enthalpy flux; the contours of wind speed are parallel to the contours of enthalpy flux in general, and the distribution of horizontal gradient of enthalpy flux is consistent with that of wind speed. Based on the strong correlation between enthalpy flux and wind speed, it can be concluded that different heat flux parameterization schemes lead to differences in sea surface heat flux, which in turn has an important impact on the intensity of typhoons.
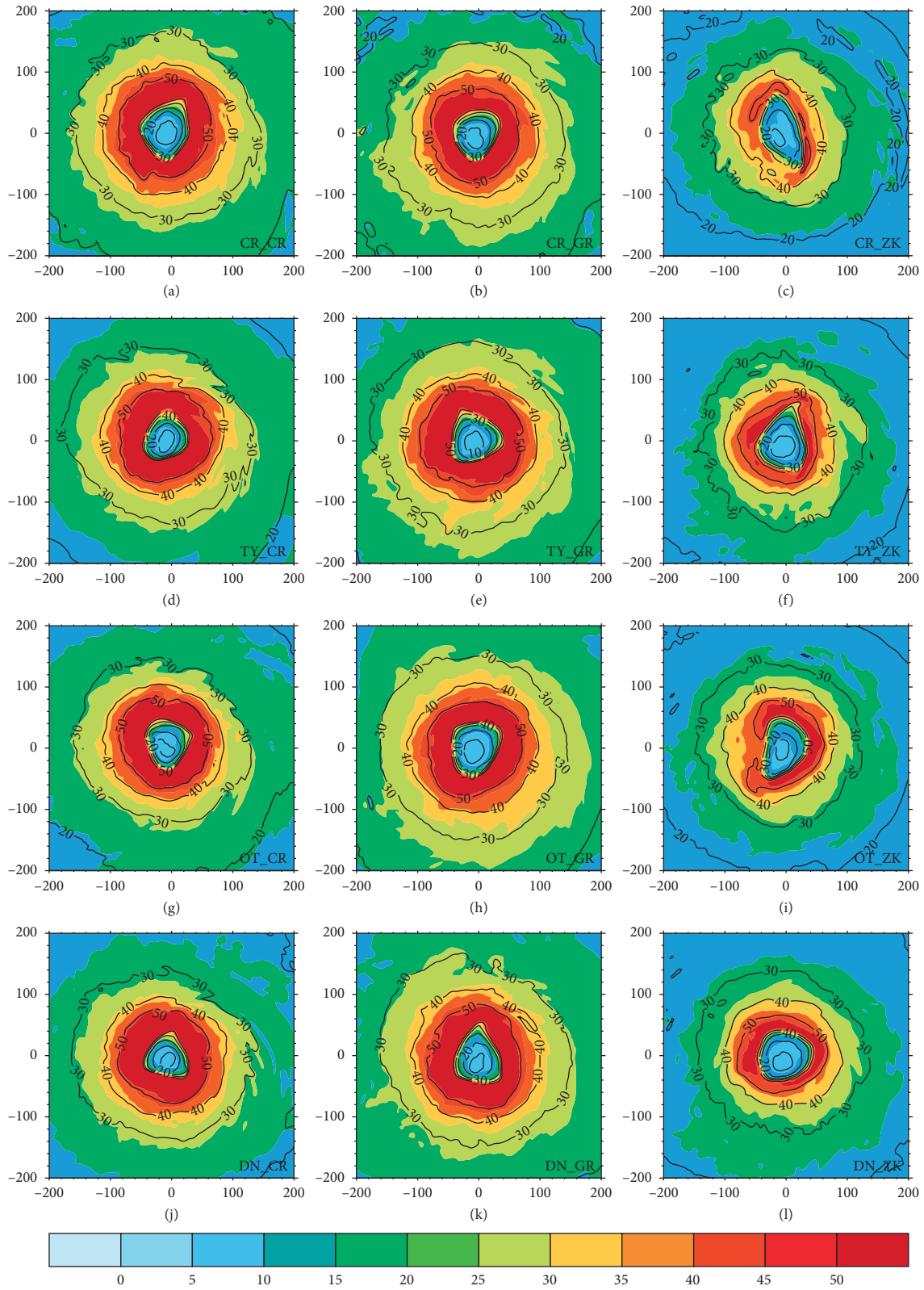
FIGURE 9: Comparison between enthalpy flux (colors, W/m^2) and wind speed at 10 m level (black lines, m/s) from 12 experiments at 1200 UTC 27 Oct 2018. Axis denotes the distance (km) from the center of the typhoon.

5. Conclusions

It is of great significance to accurately forecast the intensity of tropical cyclones, especially typhoons. Energy transfer between air and sea is crucial for the evolution of typhoon intensity. In this paper, we use the coupling model COAWST to study the impacts of four momentum flux parameterization schemes and three heat flux parameterization schemes on the simulation of Super Typhoon Yutu. From the results, we concluded the following.

(1) Track simulations of Yutu are not sensitive to the flux parameterization schemes. Differences between schemes are mainly presented in the intensity simulations. Among the four momentum flux parameterization schemes, three wave-state-based schemes (TY, OT, and DN) provide better intensity results than the wind-speed-based COARE scheme. This is caused by the different performances of them in parameterization of z_0. Three wave-state-based schemes (TY, OT, and DN) provide better intensity results than the wind-speed-based COARE scheme because wave state has a nonnegligible impact on the sea surface roughness.

(2) Among the three heat flux parameterization schemes, the results of the GR scheme are slightly better than that of the COARE scheme; both the GR and COARE schemes are significantly better than the ZK scheme, from which the intensity of Yutu is under predicted obviously. The poor result of ZK is because it calculates an unreasonable z_t and z_q. The enthalpy exchange coefficient calculated by ZK decreases with increasing wind speed, which is not consistent with the consensus that enthalpy exchange coefficient increases or keeps constant with increasing wind speed.

(3) Differences of intensity between different schemes are related to the simulated sea surface heat flux. Heat transferred at sea surface has a significant impact on the wind field. There is a strong correlation between the distributions of wind speed and distributions of enthalpy flux; area with large enthalpy flux can acquire more energy from the ocean, which leads to the development of wind field.

Data Availability

The JTWC TC Best-Track data used to support the findings of this study have been deposited in the Joint Typhoon Warning Center website (https://www.metoc.navy.mil/jtwc/jtwc.html?western-pacific). The NCEP analysis data are obtained from https://rda.ucar.edu/datasets/ds083.3/.

Conflicts of Interest

The authors declare that they have no conflicts of interest.

References

[1] X. Lyu, X. Wang, and L. M. Leslie, "The dependence of Northwest Pacific tropical cyclone intensification rates on environmental factors," *Advances in Meteorology*, vol. 201918 pages, Article ID 9456873, 2019.

[2] T. Hu, B. Liu, D. Wu, and X. Yi, "Analysis of the gale in the bohai sea caused by tropical cyclone Yagi," *Advances in Meteorology*, vol. 2019, Article ID 1853797, 15 pages, 2019.

[3] Y. Chen, F. Zhang, B. W. Green, and X. Yu, "Impacts of ocean cooling and reduced wind drag on Hurricane Katrina (2005) based on numerical simulations," *Monthly Weather Review*, vol. 146, no. 1, pp. 287–306, 2018.

[4] J.-W. Bao, S. A. Michelson, and J. M. Wilczak, "Sensitivity of numerical simulations to parameterizations of roughness for surface heat fluxes at high winds over the sea," *Monthly Weather Review*, vol. 130, no. 7, pp. 1926–1932, 2002.

[5] G. H. Bryan, "Effects of surface exchange coefficients and turbulence length scales on the intensity and structure of numerically simulated hurricanes," *Monthly Weather Review*, vol. 140, no. 4, pp. 1125–1143, 2012.

[6] B. W. Green and F. Zhang, "Impacts of air-sea flux parameterizations on the intensity and structure of tropical cyclones," *Monthly Weather Review*, vol. 141, no. 7, pp. 2308–2324, 2013.

[7] S. Liu, J. Li, L. Sun et al., "Basin-wide responses of the south China sea environment to super typhoon mangkhut (2018)," *Science of The Total Environment*, vol. 731, Article ID 139093, 2020.

[8] S. D. Smith, R. J. Anderson, W. A. Oost et al., "Sea surface wind stress and drag coefficients: the HEXOS results," *Boundary-Layer Meteorology*, vol. 60, no. 1-2, pp. 109–142, 1992.

[9] G. L. Geernaert, S. E. Larsen, and F. Hansen, "Measurements of the wind stress, heat flux, and turbulence intensity during storm conditions over the North Sea," *Journal of Geophysical Research*, vol. 92, no. C12, pp. 13127–13139, 1987.

[10] J. B. Edson, V. Jampana, R. A. Weller et al., "On the exchange of momentum over the open ocean," *Journal of Physical Oceanography*, vol. 43, no. 8, pp. 1589–1610, 2013.

[11] B. Liu, C. Guan, and L. Xie, "The wave state and sea spray related parameterization of wind stress applicable from low to extreme winds," *Journal of Geophysical Research: Oceans*, vol. 117, no. C11, 2012.

[12] D. Zhao and M. Li, "Dependence of wind stress across an air-sea interface on wave states," *Journal of Oceanography*, vol. 75, no. 3, pp. 207–223, 2019.

[13] J. Kondo, "Air-sea bulk transfer coefficients in diabatic conditions," *Boundary-Layer Meteorology*, vol. 9, no. 1, pp. 91–112, 1975.

[14] J. Wu, "Wind-Stress coefficients over sea surface near neutral conditions-A revisit," *Journal of Physical Oceanography*, vol. 10, no. 5, pp. 727–740, 1980.

[15] W. G. Large and S. Pond, "Open ocean momentum flux measurements in moderate to strong winds," *Journal of Physical Oceanography*, vol. 11, no. 3, pp. 324–336, 1981.

[16] M. A. Donelan, "The dependence of the aerodynamic drag coefficient on wave parameters," in *Proceedings of First International Conference on Meteorology and Air-Sea Interaction of the Coastal Zone*, pp. 381–387, Hague, Netherlands, May 1982.

[17] D. Vickers and L. Mahrt, "Fetch limited drag coefficients," *Boundary-Layer Meteorology*, vol. 85, no. 1, pp. 53–79, 1997.

[18] W. M. Drennan, H. C. Graber, and M. A. Donelan, "Evidence for the effects of swell and unsteady winds on marine wind stress," *Journal of Physical Oceanography*, vol. 29, no. 8, pp. 1853–1864, 1999.

[19] C. Guan and L. Xie, "On the linear parameterization of drag coefficient over sea surface," *Journal of Physical Oceanography*, vol. 34, no. 12, pp. 2847–2851, 2004.

[20] A. Toffoli, L. Loffredo, P. Le Roy, J.-M. Lefèvre, and A. Babanin, "On the variability of sea drag in finite water depth," *Journal of Geophysical Research: Oceans*, vol. 117, no. C11, 2012.

[21] M. A. Bender, I. Ginis, and Y. Kurihara, "Numerical simulations of tropical cyclone-ocean interaction with a high-resolution coupled model," *Journal of Geophysical Research*, vol. 98, no. D12, pp. 23245–23263, 1993.

[22] H. L. Tolman, B. Balasubramaniyan, L. D. Burroughs et al., "Development and implementation of wind-generated ocean surface wave modelsat NCEP," *Weather and Forecasting*, vol. 17, no. 2, pp. 311–333, 2002.

[23] M. Donelan, B. K. Haus, N. Reul et al., "On the limiting aerodynamic roughness of the ocean in very strong winds," *Geophysical Research Letters*, vol. 31, no. 18, 2004.

[24] N. Takagaki, S. Komori, N. Suzuki et al., "Strong correlation between the drag coefficient and the shape of the wind sea spectrum over a broad range of wind speeds," *Geophysical Research Letters*, vol. 39, no. 23, 2012.

[25] M. D. Powell, P. J. Vickery, and T. A. Reinhold, "Reduced drag coefficient for high wind speeds in tropical cyclones," *Nature*, vol. 422, no. 6929, pp. 279–283, 2003.

[26] Y. Troitskaya, E. Ezhova, I. Soustova, and S. Zilitinkevich, "On the effect of sea spray on the aerodynamic surface drag under severe winds," *Ocean Dynamics*, vol. 66, no. 5, pp. 659–669, 2016.

[27] S. Komori, K. Iwano, N. Takagaki et al., "Laboratory measurements of heat transfer and drag coefficients at extremely high wind speeds," *Journal of Physical Oceanography*, vol. 48, no. 4, pp. 959–974, 2018.

[28] P. K. Taylor and M. J. Yelland, "The dependence of sea surface roughness on the height and steepness of the waves," *Journal of Physical Oceanography*, vol. 31, no. 2, pp. 572–590, 2001.

[29] W. M. Drennan, H. C. Graber, D. Hauser, and C. Quentin, "On the wave age dependence of wind stress over pure wind seas," *Journal of Geophysical Research: Oceans*, vol. 108, no. C3, 2003.

[30] Z. Ma, J. Fei, X. Huang, X. Cheng, and L. Liu, "A study of the interaction between typhoon francisco (2013) and a cold-core eddy. part ii: boundary layer structures," *Journal of the Atmospheric Sciences*, vol. 77, no. 8, pp. 2865–2883, 2020.

[31] Y. Zhang, Z. Zhang, D. Chen, B. Qiu, and W. Wang, "Strengthening of the kuroshio current by intensifying tropical cyclones," *Science*, vol. 368, no. 6494, pp. 988–993, 2020.

[32] J. DeCosmo, K. B. Katsaros, S. D. Smith et al., "Air-sea exchange of water vapor and sensible heat: the Humidity Exchange over the Sea (HEXOS) results," *Journal of Geophysical Research: Oceans*, vol. 101, no. C5, pp. 12001–12016, 1996.

[33] V. Bharti, C. W. Fairall, B. W. Blomquist et al., "Air-sea heat and momentum fluxes in the southern ocean," *Journal of Geophysical Research: Atmospheres*, vol. 124, no. 23, pp. 12426–12443, 2019.

[34] S. S. Zilitinkevich, A. A. Grachev, and C. W. Fairall, "NOTES and CORRESPONDECEScaling reasoning and field data on the sea surface roughness lengths for scalars," *Journal of the Atmospheric Sciences*, vol. 58, no. 3, pp. 320–325, 2001.

[35] P. J. Webster and R. Lukas, "TOGA COARE: Toga COARE: the Coupled Ocean-atmosphere Response experiment," *Bulletin of the American Meteorological Society*, vol. 73, no. 9, pp. 1377–1416, 1992.

[36] A. B. Villas Boas, F. Ardhuin, A. Ayet et al., "Integrated observations and modeling of global winds, currents, and waves: requirements and challenges for the next decade," *Frontiers in Marine Science*, vol. 6, p. 425, 2019.

[37] A. Yool, J. Palmiéri, C. Jones et al., "Spin-up of UK earth system model 1 (UKESM1) for CMIP6," *Journal of Advances in Modeling Earth Systems*, vol. 12, no. 8, p. e2019MS001933, 2020.

[38] H. Charnock, "Wind stress on a water surface," *Quarterly Journal of the Royal Meteorological Society*, vol. 81, no. 350, pp. 639-640, 1955.

[39] S. D. Smith, K. B. Katsaros, W. A. Oost, and P. G. Mestayer, "Two major experiments in the humidity exchange over the sea (HEXOS) program," *Bulletin of the American Meteorological Society*, vol. 71, no. 2, pp. 161–172, 1990.

[40] L. Mahrt, D. Vickers, J. Howell et al., "sea surface drag coefficients in the Risø Air Sea experiment," *Journal of Geophysical Research: Oceans*, vol. 101, no. C6, pp. 14327–14335, 1996.

[41] F. Anctil and M. A. Donelan, "Air-water momentum flux observations over shoaling waves," *Journal of Physical Oceanography*, vol. 26, no. 7, pp. 1344–1353, 1996.

[42] W. A. Oost, G. J. Komen, C. M. J. Jacobs, and C. Van Oort, "New evidence for a relation between wind stress and wave age from measurements during ASGAMAGE," *Boundary-Layer Meteorology*, vol. 103, no. 3, pp. 409–438, 2002.

[43] M. Donelan and W. Drennan, "Direct field measurements of the flux of carbon dioxide," *Air-Water Gas Transfer*, vol. 677, p. 683, 1995.

[44] D. Hauser, H. Branger, S. Bouffies-Cloché et al., "The FETCH experiment: an overview," *Journal of Geophysical Research: Oceans*, vol. 108, no. C3, 2003.

[45] M. A. Donelan, W. M. Drennan, and K. B. Katsaros, "The air-sea momentum flux in conditions of wind sea and swell," *Journal of Physical Oceanography*, vol. 27, no. 10, pp. 2087–2099, 1997.

[46] M. A. Donelan, N. Madsen, K. K. Kahma, I. K. Tsanis, and W. M. Drennan, "Apparatus for atmospheric surface layer measurements over waves," *Journal of Atmospheric and Oceanic Technology*, vol. 16, no. 9, pp. 1172–1182, 1999.

[47] J. R. Garratt, "The atmospheric boundary layer," *Earth-Science Reviews*, vol. 37, no. 1-2, pp. 89–134, 1994.

[48] C. W. Fairall, A. B. White, J. B. Edson, and J. E. Hare, "Integrated shipboard measurements of the marine boundary layer," *Journal of Atmospheric and Oceanic Technology*, vol. 14, no. 3, pp. 338–359, 1997.

[49] J. C. Warner, B. Armstrong, R. He, and J. B. Zambon, "Development of a Coupled Ocean-Atmosphere-Wave-Sediment transport (COAWST) modeling system," *Ocean Modelling*, vol. 35, no. 3, pp. 230–244, 2010.

[50] Z. Liwei and Z. Tianjun, "A review of development and application of regional ocean-atmosphere coupled model," *Advances in Earth Science*, vol. 27, no. 8, pp. 857–865, 2012.

[51] S.-H. Chen and W.-Y. Sun, "A one-dimensional time dependent cloud model," *Journal of the Meteorological Society of Japan. Ser. II*, vol. 80, no. 1, pp. 99–118, 2002.

[52] M. J. Iacono, J. S. Delamere, E. J. Mlawer et al., "Radiative forcing by long-lived greenhouse gases: calculations with the AER radiative transfer models," *Journal of Geophysical Research: Atmospheres*, vol. 113, no. D13, 2008.

[53] M. Nakanishi and H. Niino, "Development of an improved turbulence closure model for the atmospheric boundary layer," *Journal of the Meteorological Society of Japan*, vol. 87, no. 5, pp. 895–912, 2009.

[54] M. Ek, K. Mitchell, Y. Lin et al., "Implementation of Noah land surface model advances in the National Centers for Environmental Prediction operational mesoscale Eta model," *Journal of Geophysical Research: Atmospheres*, vol. 108, no. D22, 2003.

[55] J. S. Kain, "The kain-fritsch convective parameterization: an update," *Journal of Applied Meteorology*, vol. 43, no. 1, pp. 170–181, 2004.

[56] M. Olabarrieta, J. C. Warner, B. Armstrong, J. B. Zambon, and R. He, "Ocean-atmosphere dynamics during Hurricane Ida and Nor'Ida: an application of the coupled ocean-atmosphere-wave-sediment transport (COAWST) modeling system," *Ocean Modelling*, vol. 43-44, pp. 112–137, 2012.

[57] J. Song, Y. Duan, and P. J. Klotzbach, "Increasing trend in rapid intensification magnitude of tropical cyclones over the western North Pacific," *Environmental Research Letters*, vol. 15, no. 8, p. 084043, 2020.

[58] H. Chen and D.-L. Zhang, "On the rapid intensification of hurricane wilma (2005). part ii: convective bursts and the upper-level warm core," *Journal of the Atmospheric Sciences*, vol. 70, no. 1, pp. 146–162, 2013.

[59] X. Tang, F. Ping, S. Yang, M. Li, and J. Peng, "Relationship between convective bursts and the rapid intensification of typhoon mujigae (2015)," *Atmospheric Science Letters*, vol. 19, no. 4, p. e811, 2018.

[60] X. Chen, Y. Yao, S. Zhao et al., "Estimation of high-resolution global monthly ocean latent heat flux from MODIS SST product and AMSR-E data," *Advances in Meteorology*, vol. 2020, Article ID 8857618, 19 pages, 2020.

[61] M. Golbazi and C. L. Archer, "Methods to estimate surface roughness length for offshore wind energy," *Advances in Meteorology*, vol. 2019, Article ID 5695481, 15 pages, 2019.

[62] W. M. Drennan, P. K. Taylor, and M. J. Yelland, "Parameterizing the sea surface roughness," *Journal of Physical Oceanography*, vol. 35, no. 5, pp. 835–848, 2005.

[63] K. R. Prakash, V. Pant, and T. Nigam, "Effects of the sea surface roughness and sea spray-induced flux parameterization on the simulations of a tropical cyclone," *Journal of Geophysical Research: Atmospheres*, vol. 124, no. 24, pp. 14037–14058, 2019.

[64] C. A. Friehe and K. F. Schmitt, "Parameterization of air-sea interface fluxes of sensible heat and moisture by the bulk aerodynamic formulas," *Journal of Physical Oceanography*, vol. 6, no. 6, pp. 801–809, 1976.

[65] D. B. Ross and V. Cardone, "Observations of oceanic whitecaps and their relation to remote measurements of surface wind speed," *Journal of Geophysical Research*, vol. 79, no. 3, pp. 444–452, 1974.

[66] G. L. Geernaert, K. B. Katsaros, and K. Richter, "Variation of the drag coefficient and its dependence on sea state," *Journal of Geophysical Research*, vol. 91, no. C6, pp. 7667–7679, 1986.